



Enhanced adsorption of Methylene blue with walnut shell carbon chemically activated by K_2CO_3

Gangxin Ren¹ · Zhiyu Li¹ · Peng Fu¹

Received: 14 February 2024 / Revised: 26 April 2024 / Accepted: 6 May 2024
© The Author(s), under exclusive licence to Springer-Verlag GmbH Germany, part of Springer Nature 2024

Abstracts

In this study, walnut shell-based activated carbon (WSAC2-900) was prepared by pyrolysis-carbonization coupled with chemical activation of K_2CO_3 for the first time. The samples were characterized by XRD, nitrogen adsorption/desorption, SEM and FTIR. In addition, the zero-point potential pH_{pzc} was determined. The specific surface area of WSAC2-900 reached $1690\text{ m}^2/\text{g}$, and the total pore volume was $0.73\text{ cm}^3/\text{g}$, of which 87.7% was the micropore volume. The surface of WSAC2-900 is rich in many oxygen-containing functional groups, such as hydroxyl and aldehyde groups, and its zero-charge point pH_{pzc} is less than 2. The isotherms, kinetics and thermodynamics of MB adsorption by WSAC2-900 were investigated. The removal efficiency of WSAC2-900 for MB reached 99.6%, and the maximum adsorption capacity reached 557.5462 mg/g . At 283 K, 293 K, 303 K and 313 K, the maximum adsorption capacities of MB were 468.1695 mg/g , 506.3057 mg/g , 524.4298 mg/g and 548.2178 mg/g , respectively. In addition, the mechanism of MB adsorption by WSAC2-900 was discussed.

Keywords Walnut shell · Activated carbon · Adsorption properties · Methylene blue

1 Introduction

One of the greatest challenges of the twenty-first century is the provision of safe drinking water to millions of people around the world, whose pollution potential is increasing as a result of rapid industrialization and the diversity of human activities. The world produces more than 8×10^5 tons of dyes every year, and approximately 200,000 tons of textile dye waste are disposed of as industrial wastewater [1–3]. Dye pollution is a potential threat to the balance between the environment and human health. Among a wide variety of pigments, MB is a heterocyclic aromatic organic compound used mainly in the dyeing of fabrics and ornaments [4, 5]. MB not only causes eye and skin stinging, similar to other dyes but also causes hypertension, mental disorders, nausea, gastrointestinal disorders and other diseases when the concentration is greater than 7.0 mg/kg [6–8]. Every year,

the state spends a large amount of money on the removal of nonferrous dye waste, and eliminating dye pollution in the environment has become an important issue.

A variety of technologies have been applied to the removal of colored dyes, including reverse osmosis [9], membrane filtration [10], biofiltration [11], coagulation/flocculation [12], chemical precipitation [13], and adsorption [14]. Compared with other technologies, adsorption is the most ideal and promising strategy for the treatment of MB in aqueous solutions due to its ease of operation, low cost and efficient removal capability [15]. In the selection of adsorbents, the use of commercial activated carbon as an adsorbent greatly increases the cost of production. Therefore, researchers are exploring the use of inexpensive and abundant environmental waste as an alternative to commercial activated carbon. Agriculture and forestry are major sources of environmental waste [16]. Currently, a wide variety of biomasses are involved in the preparation of activated carbon, such as palm fibre/palm husk [17, 18], coconut husk [19], walnut husk [20], corn straw [21], rice husk [22], olive stone [23], cellulosic pumpkin seed hulls [24], wood shavings [25], bamboo [26], crab shells [27], and shrimp shells [28]. The transformation of agricultural wastes into high-value activated carbon provides a new way to treat agricultural wastes.

✉ Zhiyu Li
lizhiyu@sdut.edu.cn

✉ Peng Fu
fupengsdut@163.com

¹ College of Agricultural Engineering and Food Science, Shandong University of Technology, Zibo 255000, Shandong, China

Walnut shell is the main agricultural waste in China, and according to statistics, China produces more than 100,000 tons of walnut shell every year [29]. Walnut shell itself has a certain adsorption capacity [30]; after it is converted into activated carbon, the adsorption capacity is further enhanced, making it an effective adsorbent; therefore, we used walnut shell as a precursor for this study. Walnut shell activated carbon moulding occurs mainly through physical activation and chemical activation in two ways. Chemical activation is one of the most common methods for developing carbon adsorbents containing different oxygen-containing functional groups (carboxyl-COOH and hydroxyl-OH) [31, 32]. At present, studies on the chemical activation of walnut shell charcoal have focused on ZnCl_2 [33], H_3PO_4 [34], and KOH [35]. For example, Aygün et al. prepared activated carbon ACW with ZnCl_2 as an activator, and its adsorption capacity for MB was 1.33 mg/g [36]. Zichao Li [37] and Zhengyan Chen [38] used H_3PO_4 and KOH as activating agents to mold walnut shell carbon, and the adsorption of MB on activated carbon reached 867.9 mg/g and 47.6190 mg/g, respectively. Although the above activators can produce large porosities and high adsorption capacities, the disadvantages of strong corrosivity, which can cause safety problems and equipment damage at high temperatures, limit their practical application [39–41]. Therefore, it is very important to develop safe, inexpensive and effective activators.

The specific surface area of activated carbon prepared from walnut shells activated by potassium carbonate was 1046.9 m^2/g , and the adsorption capacity for mercury ions was 182.9 mg/g [42]. Using corn straw as a raw material, Ling Zhu et al. prepared potassium carbonate-activated biomass carbon KBC750, which has a maximum specific surface area of 815 m^2/g and a naphthalene adsorption capacity of 130.7 mg/g [43]. Therefore, potassium carbonate has great potential for the preparation of adsorptive activated carbon. At present, there is still a gap in the study of MB adsorption by activated carbon (WSAC) prepared from walnut shells activated by potassium carbonate. Due to the low cost, nontoxicity, and slight or noncorrosive advantages of potassium carbonate, we used potassium carbonate as an activator and Walnut shell as a precursor. WSAC, a walnut shell activated carbon with a high specific surface area and rich micropore structure, was successfully prepared by a two-step heating method. The effects of the activation temperature and impregnation ratio on the structure and adsorption properties of activated carbon were compared. The samples were characterized by XRD, nitrogen adsorption/desorption, SEM and FTIR. In addition, the zero-point potential pH_{pzc} was determined. The activated carbon sample WSAC2-900, with the highest parameters, was used as the adsorbent. The effects of different initial concentrations of MB solution, pH values of the solution, contact times and

temperatures on the adsorption performance were studied, and the optimum adsorption conditions for WSAC2-900 were determined. The isotherms, kinetics and thermodynamics of MB adsorption by WSAC2-900 were investigated. In addition, the mechanism of MB adsorption by WSAC2-900 was discussed.

2 Materials and methods

2.1 Chemicals and instruments

The analytical grade cationic dyes methylene blue (MB) ($\geq 98.5\%$), NaOH ($\geq 96\%$), HCl (99%), K_2CO_3 (analytical purity $\geq 99\%$, provided by Sinopharm Chemical Reagent Co., Ltd.), anhydrous ethanol (Yantai Shuangshuang Chemical Co., Ltd.), and walnut shells were produced and grown locally in Zibo. The equipment used included a tubular furnace (Tianjin Zhonghuan Electric Furnace Co., Ltd.), a UV–visible spectrophotometer, a pH meter, a thermostatic water bath shaker, an electric thermostatic drying oven (Shaoxing Shangcheng Instrument Manufacturing Co., Ltd.), a BET surface area and pore size analyser (Micromeritics - ASAP2460, USA), Fourier transform infrared spectroscopy (FT-IR) (Thermo Fisher Scientific - Nicolet IS5, USA), and a liquid zeta particle size/potential analyser (Dynamic Light Scattering, DLS) (Malvern - Zetasizer Nano S90, UK).

2.2 Preparation of walnut shell carbon

The walnut shells were washed with ultrapure water, dried, ground into powder, and sieved. The dried WSAC was pyrolyzed in a tubular furnace at 400 °C for 4 hours (heating rate of 5 °C/min, nitrogen intake rate of 150 mL/min) and then cooled to room temperature to obtain biochar. Subsequently, 4 g of WSAC and 8 g of K_2CO_3 were thoroughly mixed, ground, and passed through a 60-mesh sieve. The mixture was then placed in a tubular furnace and heated at 900 °C for 2 hours in a nitrogen atmosphere (heating rate of 10 °C/min, N_2 flow rate of 150 mL/min) [44]. Finally, the resulting material was ground and passed through a 60-mesh sieve, washed alternately with dilute HCl and deionized water until the pH was neutral, and then dried at 65 °C. The product was named WSACR-T, where R represents the mass ratio of K_2CO_3 to BC ($R = 1, 2, \text{ and } 3$) and T represents the second-stage pyrolysis temperature ($T = 500, 700, \text{ and } 900^\circ\text{C}$).

2.3 Characterization

The pore structure characteristics of the activated carbon were analysed using a BET surface area and pore size analyser (Micromeritics - ASAP2460, USA). N_2 adsorption and desorption isotherms were measured at 77 K. The

micromorphology of the activated carbon was observed using a scanning electron microscope (SEM) (ZEISS - Sigma 500, Germany). After sputter coating with gold using a sputtering device, SEM images were obtained in the range of 100 μm to 1 μm under an accelerating voltage of 30 kV. Before and after MB adsorption, the changes in the chemical groups of WSAC2-900 were determined using Fourier transform infrared spectroscopy (FTIR) (Bruker - INVENIO S). FTIR spectra of the samples were collected in the range of 4000–400 cm^{-1} with 16 accumulated scans at a resolution of 4 cm^{-1} . The zeta potential of WSAC2-900 in the pH range of 2–10 was measured using a Zetasizer Nano S90 (Malvern, UK). By calibrating the point of zero charge (pH_{pzc}), the variation pattern of the surface charge of WSAC2-900 with the pH of the solution was summarized.

2.4 Adsorption performance

A specific amount of dried WSAC2-900 was added to 25 ml of methylene blue (MB) solution at a concentration of 400 mg/L. The adsorption process parameters were optimized by varying the pH of the MB solution (2–10), temperature (283 K–313 K), contact time (10, 20, 100–600 min), and concentration of the MB solution (50–400 mg/L). The pH of the solution was adjusted using dilute HCl and NaOH solutions. The experiments were conducted in 30 ml centrifuge tubes, which were agitated at 250 rpm. The solution was then centrifuged, and the supernatant was extracted to measure the change in MB concentration using a UV spectrophotometer (UV, U-3900, Hitachi, Japan). The tests were repeated three times to obtain average values. The removal percentage (%R) and adsorption capacity (q , mg/g) of WSAC2-900 for the MB solution were calculated using formulas (1) and (2), where C_0 and C_i represent the initial and final concentrations of MB, respectively, m is the mass of the activated carbon (g), and V is the volume of the MB solution (mL).

$$R(\%) = \left[\frac{C_0 - C_i}{C_0} \right] \times 100\% \quad (1)$$

$$q = \left[\frac{C_0 - C_i}{m} \right] \times V \quad (2)$$

2.5 Theoretical studies

2.5.1 Adsorption kinetics

Batch adsorption experiments were conducted at different time intervals on WSAC2-900 to determine the adsorption process involved. The adsorption data obtained at different

times were processed using the pseudo-first-order Lagergren equation (pseudo-first-order, PFO; kinetic model, 1898), the pseudo-second-order Lagergren equation (pseudo-second-order, PSO; kinetic model, 1999), and the intraparticle diffusion equation (referred to as IPD). The best kinetic model was selected based on the regression correlation coefficient (R^2) and the size of the adsorption capacity to determine the kinetic adsorption mechanism. The linear mathematical forms of the PFO, PSO, and IPD kinetic models are as follows (Eqs. 3, 4, 5):

$$q_t = q_e (1 - e^{-k_1 t}) \quad (3)$$

$$q_t = \frac{q_e^2 k_2 t}{1 + q_e k_2 t} \quad (4)$$

$$q_t = k_{pi} t^{1/2} + C \quad (5)$$

where:

t contact time (min)

q_t quantity of adsorbate at time t (mg/g)

q_e quantity of adsorbate at equilibrium (mg/g)

K_1 pseudo-first-order rate constant, min^{-1}

K_2 pseudo-second-order rate constant, $\text{g}/(\text{mg}\cdot\text{min})$

Generally, the closer the regression correlation coefficient (R^2) of a model is to 1, the better it explains the adsorption mechanism. The pseudo-first-order kinetic model suggests that the rate-limiting step in adsorption is the internal diffusion resistance within the particles, while the pseudo-second-order reaction kinetic model considers that the rate-limiting factor is the adsorption mechanism itself [45]. In most cases, the PSO (pseudo-second-order) kinetic model is most suitable for processes involving dye adsorption.

2.5.2 isotherm adsorption

Isotherm adsorption models are used to study the relationship between the amount of adsorbate adsorbed on the surface of biomass activated carbon (q_e) and the equilibrium concentration of the adsorbate in the solution (C_e). By fitting and analysing the isotherms, the interaction between the biomass activated carbon and the adsorbate was clarified. Adsorption isotherm models are used to help identify the adsorption mechanism and to determine the

maximum adsorption capacity of the adsorbent. The Langmuir (1917), Freundlich (1906), Temkin and D-R isotherm models are frequently used. These sorption isotherm models were used to analyse equilibrium adsorption data for different MB concentrations. According to the Langmuir adsorption isotherm model, the adsorbent surface is considered uniform, with indistinguishable adsorption sites; all adsorbing particles have the same heat and energy; adsorption occurs in a monolayer, and there are no interactive forces between the adsorption sites and the adsorbate.

The following is the linear mathematical form of the Langmuir isotherm model:

$$q_e = \frac{bq_m C_e}{1 + bC_e} \quad (6)$$

$$R_L = \frac{1}{1 + K_L g C_i} \quad (7)$$

In this context, b is the Langmuir constant ($L \cdot mg^{-1}$), and q_{max} represents the maximum adsorption capacity. R_L is the Langmuir separation factor, which indicates the favourability of adsorption: $R_L > 1$ implies unfavourable adsorption; $R_L = 1$ indicates linear adsorption; $R_L = 0$ represents irreversible adsorption; and $0 < R_L < 1$ suggests favourable adsorption. Specifically, when $0 < R_L < 1$, the larger the value of R_L is, the more favourable it is for pollutant removal [46].

The Freundlich adsorption isotherm model represents multilayer adsorption and is an empirical model. This model assumes that the adsorbent surface is heterogeneous and that the adsorption process of the adsorbate on the adsorbent and between adsorbate molecules involves various conditions. Equation (8) displays the linear mathematical form of the Freundlich isotherm. By performing a linear fit with the experimental data, using $\ln C_e$ as the x-axis and $\ln q_e$ as the y-axis, the values of k and n in the Freundlich model are determined.

$$q_e = kC_e^{1/n} \quad (8)$$

where

n Freundlich constant related to the adsorption intensity of biomass activated carbon;

K an empirical constant related to the nature and type of pollutants in the solution and biomass activated carbon. The value of 'n' indicates the adsorbability; the larger the value of 'n', the stronger the interaction between the adsorbate and the adsorbent ($n > 1$ indicates favourable adsorption conditions) [47].

The Temkin sorption isotherm model is used to study the linear relationship between the heat of adsorption and temperature. This approach is suitable for chemical adsorption processes where the heat of adsorption varies linearly with the degree of surface coverage. The Temkin sorption isotherm model can be expressed as:

$$q_e = A \ln A_T + A \ln C_e \quad (9)$$

$$A = \frac{RT}{b} \quad (10)$$

- q_e The equilibrium adsorption capacity of biomass activated carbon, mg/g;
- R gas constant, 8.314 J/(mol·K);
- T Absolute temperature, K;
- b A constant related to the free energy of adsorption, mol^2/J^2 ;
- C_e The solubility of methylene at adsorption equilibrium, mg/g;
- A A constant relating to the heat of adsorption, L/g;
- A_T Dimensionless adsorption constant;

The Dubinin–Radushkevich model is often used to analyse adsorption mechanisms. It is assumed that the adsorption energy on the surface of the material is nonuniformly distributed and that the energy is Gauss distributed. The D-R isotherm model for the adsorption of colored dye pollutants in water by biomass activated carbon can be expressed as:

$$q_e = q_m e^{(-k\varepsilon^2)} \quad (11)$$

$$\varepsilon = RT \ln \left(1 + \frac{1}{C_e} \right) \quad (12)$$

- ε Polanyi potential energy, J/mol;
- k Parameters related to the adsorption energy, mol^2/kJ ;
- β Parameters related to the free energy of adsorption, mol^2/J^2 ;
- E Energy per mole of adsorbent, kJ/mol, $E = \frac{1}{\sqrt{2K}}$.

When $E < 8$ kJ/mol, physical adsorption occurs; when 8 kJ $< E < 16$ kJ, ion exchange occurs; and when $E > 16$ kJ, chemical adsorption occurs.

2.5.3 Thermodynamic studies

To study the spontaneous adsorption properties of MB on WSAC2-900 activated carbon, MB adsorption experiments were conducted with temperature as the single variable. The

adsorption thermodynamic parameters were calculated using the van't Hoff equation.

$$K_L = \frac{q_e}{C_e} \quad (13)$$

$$\Delta G^\circ = -RT \ln K_L \quad (14)$$

$$\ln K_L = \frac{\Delta S^\circ}{R} - \frac{\Delta H^\circ}{RT} \quad (15)$$

The slope and intercept of the linear plot of $\ln K_L$ versus $1/T$ yield the values of ΔH° and ΔS° , respectively.

3 Results and conclusions

3.1 Characterization of the physical and chemical properties of activated carbon

3.1.1 Study on the structure of activated carbon

After the activation of potassium carbonate, the crystal structure of the activated carbon was determined by X-ray diffraction (XRD). The XRD patterns of the activated carbon before and after activation are shown in Fig. 1. The WSAC2-900 sample did not show sharp diffraction peaks, indicating that cleaning with hydrochloric acid removes potassium-containing impurities generated during the decomposition of potassium carbonate [41]. The peak position of WSAC2-900 moves forward and becomes wider than that before activation, which indicates that carbon reacts with potassium carbonate during activation. Two broad peaks were detected at $2\theta = 20.64^\circ$ and 43.68° after activation, which are attributed to the (002) and (100) planes in the disordered carbon material structure due to graphite disorder [48, 49]. The XRD results show that the activated carbon is amorphous. The increase in the peak intensity indicates that the activation of potassium carbonate promoted the formation of graphite structures [50].

Figure 2a shows the N_2 sorption isotherms of activated carbon prepared at different impregnation ratios and at different temperatures. The image shows that there is significant N_2 adsorption in the range of 0-0.1 relative pressure, with the adsorption amount rapidly increasing at relatively low pressures and reaching a saturation point, resembling the Langmuir type adsorption isotherm. According to the IUPAC classification, WSAC2-900 has type I microporous isotherms, with all the activated carbons exhibiting characteristics of microporous solids. Table 1 summarizes the main data associated with the porous structure, and the combination of low S_{EXT} values and high V_{micro} values confirms a minor contribution from mesopores [51]. Figure 2(b-d) shows the pore size distribution of WSAC2-900,

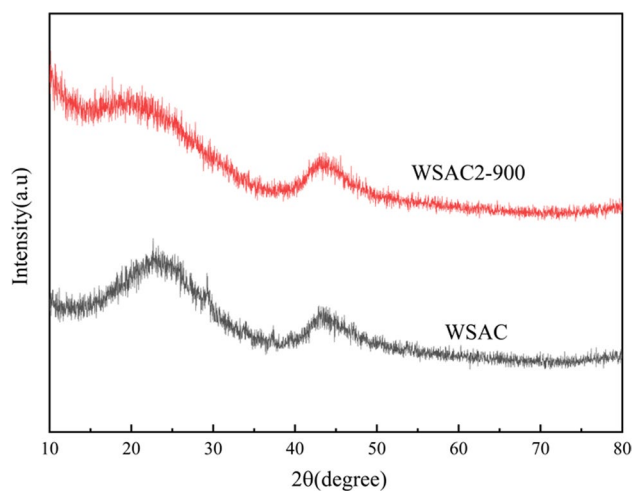


Fig. 1 XRD patterns of the WSAC and WSAC2-900 samples in the range of $2\theta = 10\text{--}80^\circ$

which has a size range of 0.7-10 μm and contains a large number of micropores as well as certain mesopores and macropores, which are advantageous for the adsorption process.

The impregnation ratio plays a critical role in the preparation of biomass activated carbon, significantly impacting the structural parameters of the activated carbon. By adjusting the impregnation ratio, it is possible to change the pore structure, optimize the adsorption activity, and introduce new functional groups, thereby enhancing the chemical reactivity of the activated carbon. Choosing an appropriate impregnation ratio is crucial for preparing activated carbon with a high specific surface area and high performance. However, a higher ratio of activator to biomass does not always lead to greater adsorption performance. Excessive impregnation ratios may result in residual chemical reagents that can destroy the already formed pore wall structures, reducing the specific surface area of activated carbon (AC). K_2CO_3 , as an activator, decomposes upon heating to produce K_2O and CO_2 , which helps in the development of micropores in the material. Additionally, the reactions of K_2CO_3 and K_2O with carbon lead to the formation of metallic potassium [52]. This potassium can diffuse into carbon layers, increasing the reactivity of carbon and producing the highly loaded activator WSAC2-900.

In addition to the impregnation ratio, temperature is another crucial factor influencing the pyrolysis effect of potassium carbonate. As the temperature increased, the specific surface area and total pore volume of the WSAC increased. At 500°C , the pore volume of the micropores is less than that of the mesopores and macropores. When the pyrolysis temperature reaches 700°C and 900°C , the pore volume and specific surface area of the micropores are greater than those of the mesopores and macropores.

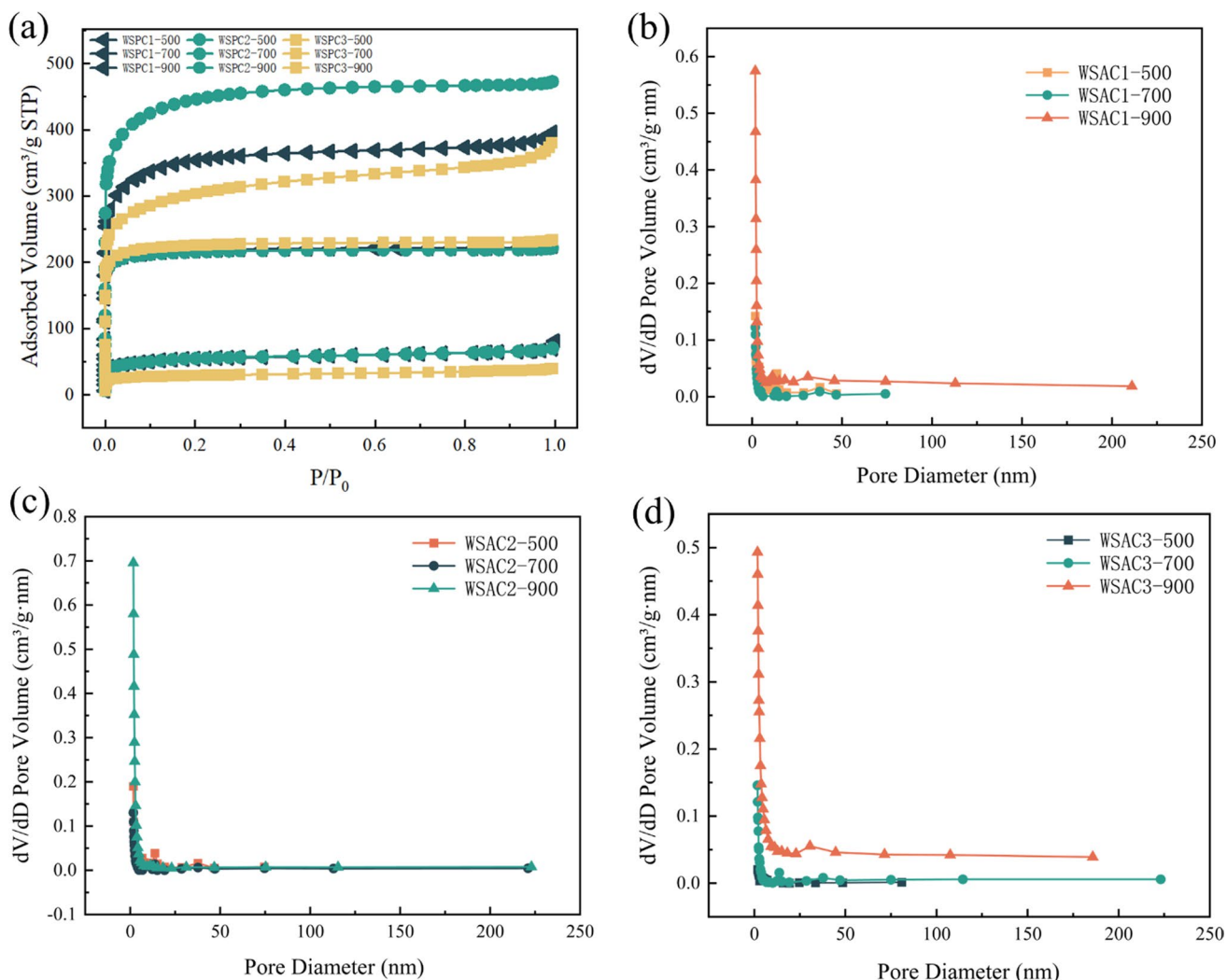


Fig. 2 Voidage structure of WSAC at different temperatures and impregnation ratios: **a** N_2 adsorption isotherms of all the ACs at -196°C . **b, c, d** Distribution of pore size of activated carbon at different temperatures and same impregnation ratio

This indicates that potassium carbonate primarily generates mesopores and macropores at lower temperatures, resulting in a lower specific surface area, while at higher temperatures, the number of micropores increases. The specific surface area increases with temperature, while the average pore size decreases with increasing activation temperature. The activated carbon WSAC2-900, which has the most developed porosity (chosen for subsequent adsorption tests), possesses a micropore volume of $0.5963\text{ cm}^3/\text{g}$ and a mesopore volume of $0.1348\text{ cm}^3/\text{g}$. The mesopore ratio is approximately 20% (percentage of mesopores relative to the total pore volume), which is considered a significant proportion for a material with a notably developed microporosity and a significant mesoporosity. Therefore, the prepared WSAC2-900, due to its significant pore structure, has the potential to

be a promising adsorbent for the adsorption of both gaseous and liquid-phase pollutants.

3.1.2 Surface morphology study

The SEM images of WSAC2-900 are shown in Fig. 3. The surface of the unactivated walnut shell carbon was relatively rough, with few pores observed Fig. 3a. The surface of WSAC2-900 became very smooth due to activation with K_2CO_3 , indicating a melted state Fig. 3b. From the longitudinal cross-section, it can be observed that the interior of the activated carbon contains abundant channels, with the carbon framework resembling a hollow lotus root structure Fig. 3c. These interconnected channels facilitate the passage of MB molecules. In the transverse cross section,

Table 1 WSAC2-900 pore structure study BET data summary

Sample	S_{BET} ($\text{m}^2\cdot\text{g}^{-1}$)	S_{EXT} ($\text{m}^2\cdot\text{g}^{-1}$)	S_{micro} ($\text{m}^2\cdot\text{g}^{-1}$)	V_{micro} ($\text{cm}^3\cdot\text{g}^{-1}$)	V_{pore} ($\text{cm}^3\cdot\text{g}^{-1}$)
WSAC1-500	198.5097	45.3591	153.1505	0.0643	0.1242
WSAC1-700	873.4205	66.9506	806.4798	0.3076	0.3482
WSAC1-900	1336.1318	162.5474	1173.5844	0.4770	0.6121
WSAC2-500	197.4769	42.7634	154.7135	0.0661	0.1091
WSAC2-700	862.2742	39.5470	822.7272	0.3160	0.3425
WSAC2-900	1690.9842	216.2026	1474.7816	0.5963	0.7311
WSAC3-500	108.3343	29.9571	78.3772	0.0316	0.0608
WSAC3-700	898.7131	64.8832	833.8299	0.3204	0.3615
WSAC3-900	1131.2337	254.8741	876.3596	0.3583	0.5874

* S_{BET} , specific surface area; S_{EXT} , external surface area; S_{micro} , microporous specific surface area; V_{micro} , microporous volume; V_{pore} , total pore volume.

WSAC2-900 has a dense internal space, resembling a honeycomb-like structure (Fig. 3d) [53]. This high porosity enhances the ability of the adsorbent to capture MB from wastewater, reducing mass transfer resistance. According to Fig. 3e, after adsorption of MB, the edges of the pore structure of the activated carbon are covered with adhesions. Upon magnification, it is evident that the surface of WSAC2-900 has increased particulate matter, with pores filled with MB particles.

3.1.3 Functional group determination and potential analysis

FTIR spectroscopy was used to further explore the surface chemical groups of WSAC2-900. The FTIR spectra of WSAC2-900 before and after the adsorption of MB are compared in Fig. 4a. New absorption bands emerged in three regions—1800–1500 cm^{-1} , 2800–3000 cm^{-1} , and 3600–3900 cm^{-1} —for WSAC2-900 after adsorption. The stretching vibration of -OH groups occurred at 3438 cm^{-1} [54], with increased vibration intensity, indicating the formation of hydrogen bonds between WSAC2-900 and MB. The antisymmetric and symmetric stretching of -CH₂ or -CH₃ in aliphatic or aliphatic groups occurred at 2920 cm^{-1} and 2851 cm^{-1} , respectively, exhibiting a decrease in aged biochar as a result of oxidation [55]. These peaks are below 3000 cm^{-1} and feature two absorption peaks, suggesting that they originate from methylene groups. The reduced transmittance

at these wavelengths before and after adsorption, along with an increase in the number of methylene groups, indicates that methylene blue was effectively attached to the surface of the activated carbon. This provides solid evidence for the study presented in this article. The amide C=O double bond can be identified by the broad band at 1631 cm^{-1} . After MB adsorption, the spectral bands shifted from 1626 and 3434 cm^{-1} to 1631 and 3440 cm^{-1} , respectively, indicating a weakened interaction between the functional groups on the surface of the activated carbon and the dye molecules. The existence of functional groups such as carboxyl groups was further confirmed using the zeta potential of WSAC2-900 at different pH values. The zeta potential graph Fig. 4b shows that the material maintains a negative charge between pH 2 and 10. When the pH is greater than 2, the surface negativity of WSAC2-900 gradually increases due to hydrolysis, thereby enhancing its adsorption capacity for cationic dyes (as shown in Fig. 7a).

3.2 Adsorption performance

3.2.1 Impact of the MB concentration and sorption isotherm

The impact of the initial concentration on the adsorption capacity of WSAC2-900 is shown in Fig. 5a. As the concentration of methylene blue (MB) increased from 50 mg/L to 400 mg/L, the adsorption capacity also increased. This is because the mass transfer between WSAC2-900 and MB molecules increases with increasing concentration, and the driving force between molecules increases, allowing MB molecules to be brought to the surface of the adsorbent more rapidly [56]. However, as effective adsorption sites gradually become occupied by the adsorbate, the adsorption quantity starts to approach an equilibrium state at approximately 250 mg/L, and the adsorption efficiency decreases. The maximum adsorption capacity of WSAC2-900 was approximately 557.5462 mg/g.

To better understand the interaction between activated carbon and MB dye molecules, the Langmuir, Freundlich, Temkin and D-R sorption isotherm models were used to analyse the experimental results. The Langmuir adsorption isotherm model is suitable for describing monolayer adsorption processes, where adsorption sites on the surface of the adsorbent are uniformly distributed, and there is no interaction between MB molecules adsorbed on adjacent sites. In contrast, the Freundlich adsorption isotherm model represents multilayer adsorption, with a nonuniform distribution of adsorption sites on the adsorbent surface, and various interactions exist between the adsorbent and MB molecules, as well as among the MB molecules themselves. The Temkin sorption isotherm model is mainly used to describe the chemical adsorption

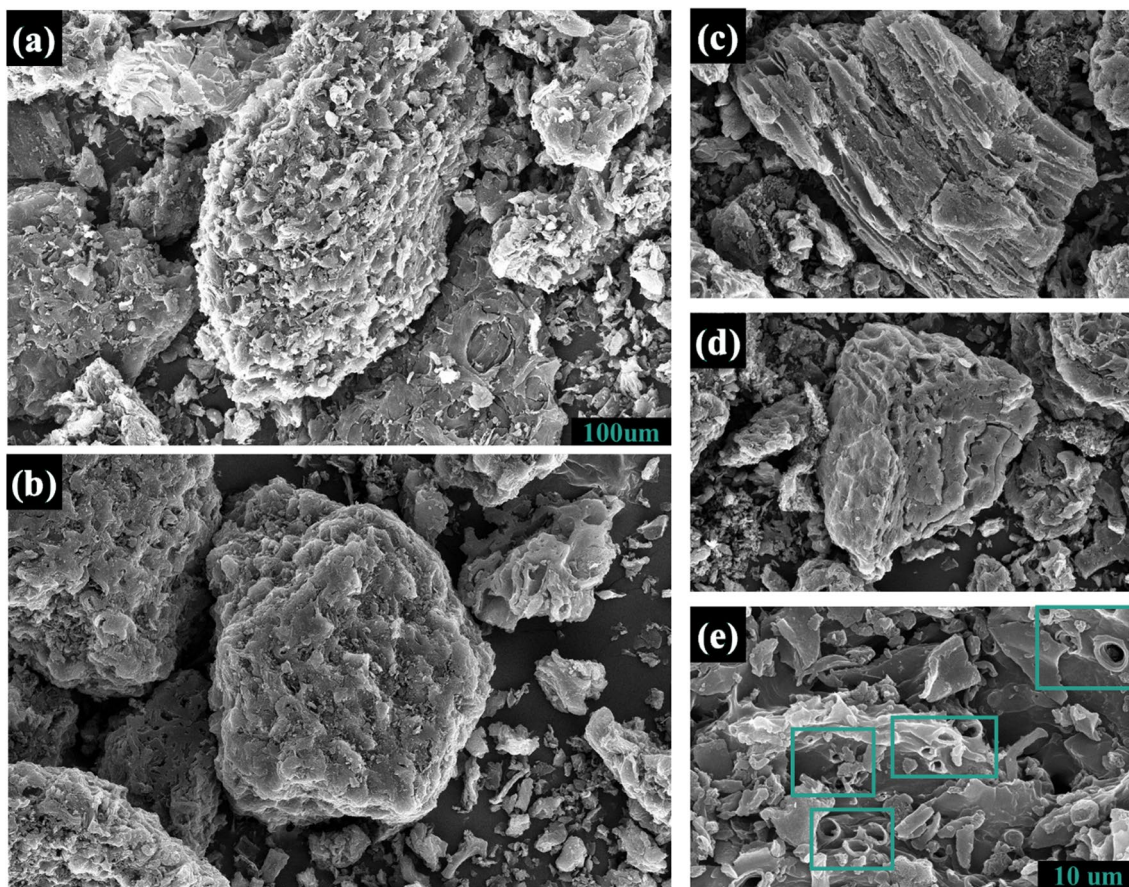


Fig. 3 Morphology and structure of WSAC2-900. SEM images: **a** Unactivated carbon WSAC-900. **b, c, d** Activated carbon sample WSAC2-900 before adsorption. **e** WSAC2-900 activated carbon after adsorption

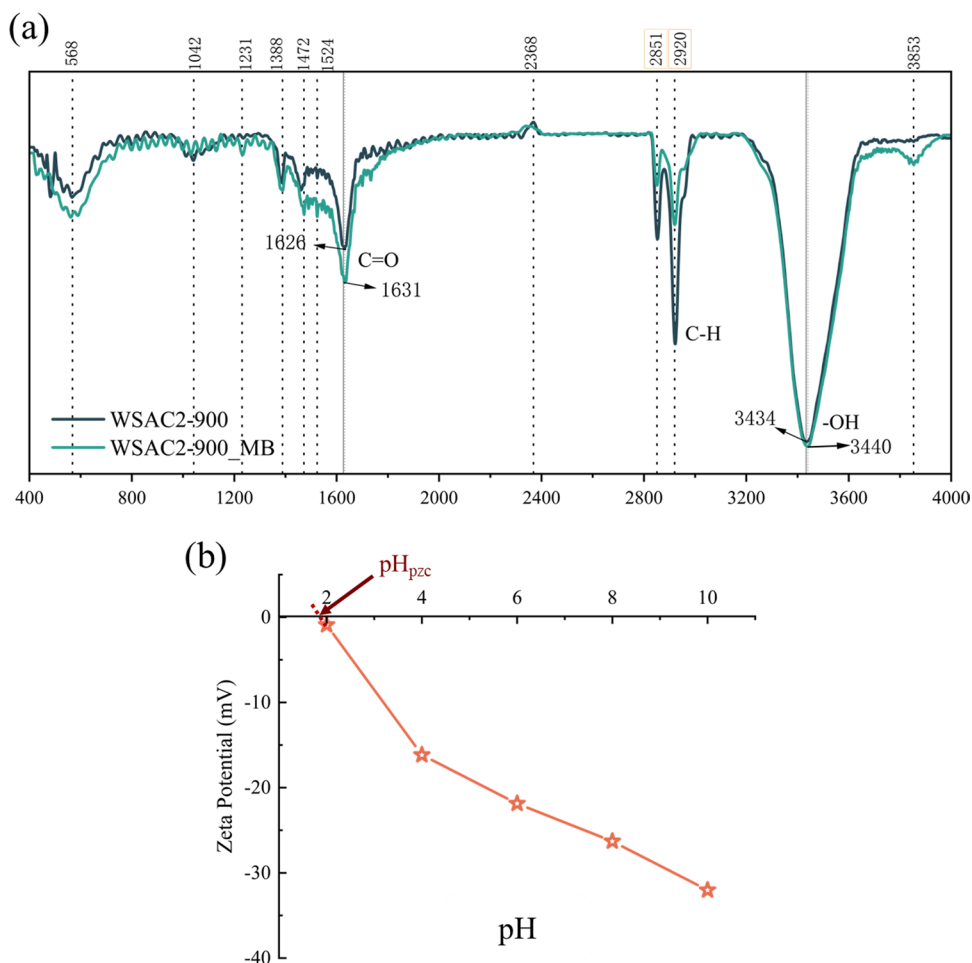
process in which the heat of adsorption varies linearly with the degree of surface coverage. The D-R sorption isotherm model is often used to analyse the adsorption mechanism, assuming that the adsorption energy is nonuniform on the surface of the material and that the energy distribution is Gaussian. According to the analysis results shown in Fig. 5(b-e), the correlation of the Langmuir isotherm ($R^2 = 0.9993$) was more significant than that of the other adsorption isotherms. The results indicate that the adsorption of MB on the WSAC2-900 surface is a process of monolayer adsorption. The results presented in Table 2 show that the adsorption equilibrium parameter R_L for methylene blue on WSAC2-900 is 0.0029, which falls within the range of 0-1. This indicates that the adsorption of MB on WSAC2-900 is advantageous and easy to occur [57]. According to the Freundlich model, the value of $1/n$ can be used as an indicator of the adsorption strength. The calculated value of $1/n$ falls between 0 and 1, indicating good adsorption characteristics on a heterogeneous surface [58]. Using the Langmuir adsorption isotherm

model, the maximum adsorption capacity of WSAC2-900 was determined to be 552.4851 mg/g, which aligns well with the actual value of 557.5462 mg/g. Compared to other activated carbons, such as coriander (296 mg/g), flax (464.2 mg/g), and bamboo charcoal (67.46 mg/g), WSAC2-900 demonstrated a greater adsorption capacity (a comparison of the adsorption capacities of different adsorbents for MB is shown in Table 3). This can be attributed to its larger specific surface area and greater porosity, as summarized in Table 1.

3.2.2 Study on the influence of contact time and adsorption kinetics

The effect of time on the adsorption capacity of WSAC2-900 was investigated at 26 °C, pH 8.13, and an MB concentration of 400 mg/L. As shown in Fig. 6a, the MB adsorption quantity rapidly increased within the first 200 minutes and then reached saturation. The maximum MB adsorption capacity of WSAC2-900 was 541.2885 mg/g.

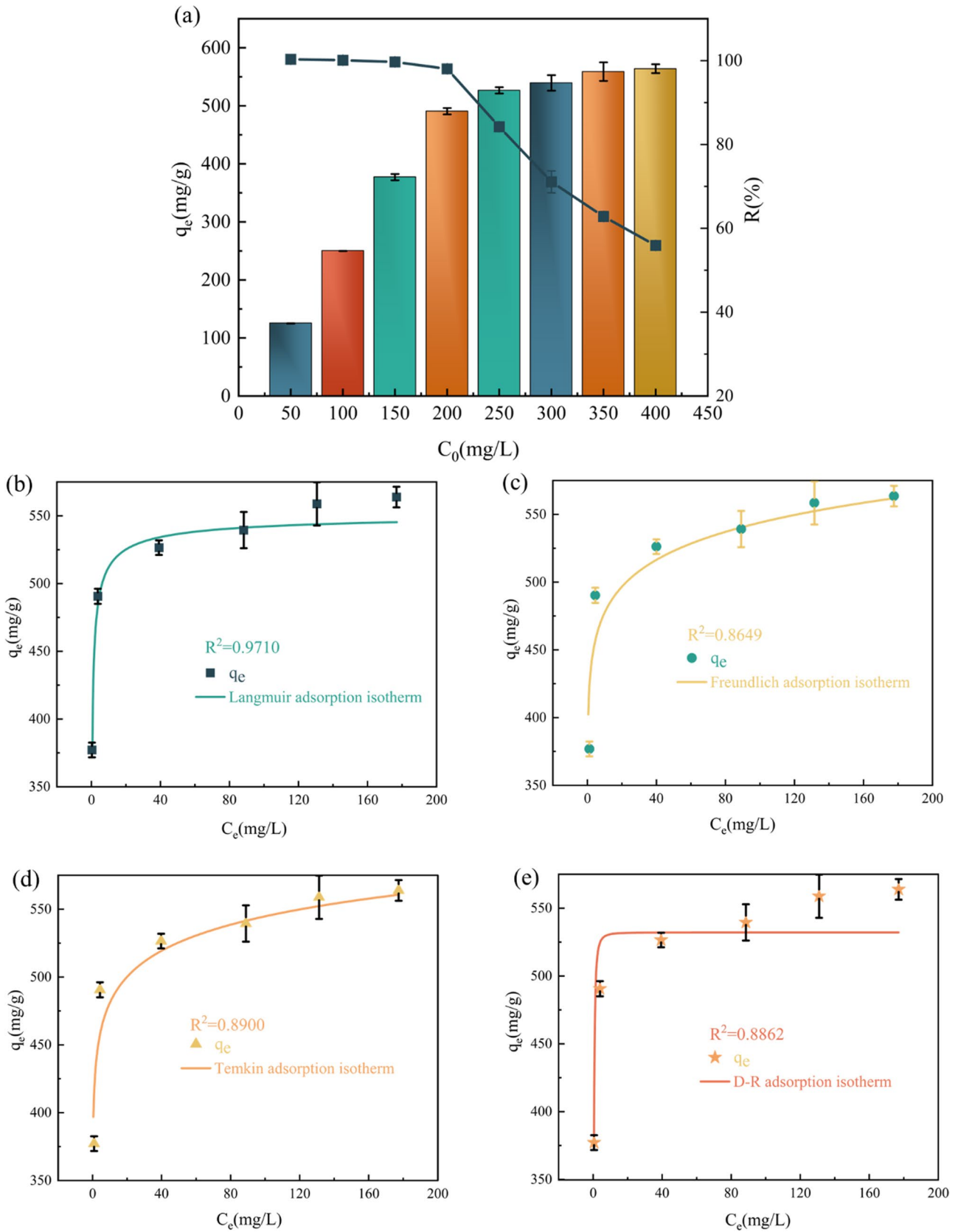
Fig. 4 Chemical characteristics of WSAC2-900: **a** FTIR spectra of WSAC2-900 before and after MB adsorption. **b** Zeta potentials of WSAC2-900 AC at different pH values



The adsorption mechanism was studied using pseudo-first-order [65], pseudo-second-order [66] and intraparticle diffusion models [67]. The correlation coefficient of the pseudo-second-order kinetic model ($R^2 = 0.9992$), as shown in Fig. 6d, was greater than that of the pseudo-first-order kinetic model ($R^2 = 0.8675$), as shown in Fig. 6c, suggesting that the pseudo-second-order kinetic model better describes the adsorption kinetics of WSAC2-900. According to the kinetic parameters presented in Table 4, the theoretical q_e value of 541.2885 mg/g from the pseudo-second-order model is consistent with the actual value of 557.5462 mg/g. This indicates that chemical adsorption occurs during this adsorption process [68]. According to the physical interpretation of the model, MB formed chemical bonds or exhibited relatively strong adsorption on the surface of WSAC2-900.

The intraparticle diffusion model was used to identify the diffusion limitations and influence of the internal structure of the particles on the overall adsorption performance during the adsorption process. From the data shown in Fig. 6b and Table 5, the in-particle diffusion model

divided the adsorption process into three linear stages, and the adsorption rate constant decreased in the order $K_{1d} > K_{2d} > K_{3d}$. This indicates that the rate of adsorption decreases over time, which is typical as the adsorption process progresses from initial rapid adsorption to slower adsorption due to fewer available sites and diffusion resistance within the particles. The first stage of adsorption is characterized primarily by surface adsorption, where the slope K_{1d} is the largest and the line segment is the steepest. This indicates that Methylene blue molecules diffuse rapidly on the surface of WSAC2-900 activated carbon during the initial stage of adsorption. This is mainly due to the synergistic effect of hydrogen bonding and electrostatic interactions. Due to the large number of oxygen-containing functional groups, a large number of potential active adsorption sites can be effectively bound to methylene blue molecules. Therefore, at this stage, chemical adsorption plays a leading role in promoting an efficient adsorption reaction. K_{2d} is the slope of the second adsorption stage, in which diffusion within the adsorbent becomes the control step due to the saturation of the adsorption sites



◀ **Fig. 5** **a** Effect of the MB concentration on the adsorption capacity of WSAC2-900 at $T = 299$ K, 10 mg of adsorbent, 25 ml of adsorbents and $\text{pH} = 8.13$. Analysis of WSAC2-900 adsorption of MB using the **b** Langmuir model, **c** Freundlich model, **d** Temkin model and **e** D-R model

on the surface and the decrease in the number of adsorption sites, and the adsorption rate decreases. In the third stage, due to the saturation of the adsorption site, diffusion within the particle becomes the dominant step, and as MB molecules need to travel a more complex path to reach the remaining small number of unoccupied active sites, the adsorption rate is further reduced. The smallest line segment of the K_{3d} value is the smoothest, indicating that the adsorption-desorption dynamic equilibrium is gradually reached in this stage [69, 70]. Additionally, the fact that the fitted straight lines do not pass through the origin confirms that intraparticle diffusion is not the sole rate-limiting factor [71, 72]. This indicates the involvement of other mechanisms in the overall adsorption process, such as surface adsorption and chemical interactions. The intercepts $C_1 < C_2 < C_3$ indicate that as time progresses, the surface of the activated carbon is increasingly occupied by MB molecules. The enhanced repulsive forces between MB molecules with the same charge, along with the reduction in available active sites, led to increased adsorption resistance. Consequently, the intercepts gradually increase until a dynamic equilibrium between adsorption and desorption is reached. This mechanism, comprising three stages, reveals the importance of the synergistic effect of external and internal diffusion during the adsorption of methylene blue onto WSAC2-900.

3.2.3 Effect of pH

With an initial MB concentration of 400 mg/L, a volume of 25 mL for MB, an adsorbent dose of 10 mg, and a temperature of 299 K, the effect of pH on the adsorption of MB by WSAC2-900 was studied by adjusting the pH using hydrochloric acid and sodium hydroxide solutions. As shown in Fig. 7a, the adsorption capacity of WSAC2-900 for MB dye increased with increasing pH from 565.4073 to 636.8153 mg/L, and no significant changes were observed above pH 8. The lower removal rate at pH 2-4 may be due to two reasons: one is the decrease in available active sites due to MB molecules and excess H^+ competing active sites on activated carbon; second, the repulsion between MB and H^+ decreases the adsorption rate. As the pH increases, the oxidative groups dissociate to form MB-oxygen binding sites that favour cationic adsorption, resulting in an increase in the number of adsorption sites and an increase in the adsorption rate [73]. Therefore, due to its cationic nature, MB

is more readily adsorbed in alkaline environments. The results indicate that a pH range of 8-10 is more conducive for adsorption experimental studies. Notably, the variation in adsorption capacity related to the initial pH suggested the existence of electrostatic interactions between WSAC2-900 and MB [74, 75].

In addition to the effect of H^+ on MB adsorption, the potential competition of coexisting cations for electrostatic sites must also be considered. As shown in Fig. 7b, common cationic perturbations, including K^+ , Na^+ , Mg^{2+} , Ca^{2+} and Fe^{3+} , were investigated. The results show that, except for Fe^{3+} , other ions have less effect on MB adsorption, indicating that the higher the valence state of interfering ions is, the more obvious the effect on MB adsorption. To better verify this phenomenon, the adsorption of WSAC2-900 on monovalent, bivalent and trivalent ions was considered only without the addition of MB, and WSAC2-900 exhibited a high removal rate of Fe^{3+} , which was basically in agreement with the results of the point-line diagram. Figure 7c shows the displacement of MB molecules by coexisting cations. An experiment was performed in a 338 K water bath in which WSAC2-900 was immersed after the complete adsorption of MB to KCl , NaCl , MgCl_2 , CaCl_2 , and FeCl_3 . In contrast to the control, the FeCl_3 solution turned green rapidly and became darker, which indicated that FeCl_3 strongly displaced the MB molecules and could desorb the MB molecules well.

3.2.4 Thermodynamic studies

Adsorption experiments of MB were conducted in the temperature range of 283 K to 313 K to investigate the thermodynamic characteristics of MB adsorption by WSAC2-900. Figure 7d shows that at 283 K, the adsorption capacity is 468.1695 mg/g, and when the temperature is increased to 313 K, the adsorption capacity reaches 548.2178 mg/g. The results show that the kinetic energy of MB increases with increasing temperature, which increases the frequency of MB molecules approaching the active sites on the surface of activated carbon and the adsorption capacity [76, 77]. The fitted curve and thermodynamic parameters were calculated by the van't Hoff equation, and the linear relationship between $\ln K_L$ and $1/T$ is shown in Fig. 7e ($R^2 = 0.9800$). The entropy change ΔS° and enthalpy change ΔH° can be obtained by calculating the intercept and slope.

According to the data analysis results from Table 6, both ΔS° and ΔH° are positive, indicating that the adsorption of MB by WSAC2-900 is an endothermic process and that the disorder of the system increases during the adsorption process, which is consistent with the general trends observed

Table 2 Summary of Langmuir, Freundlich, Temkin, and DR isotherm model parameters for the adsorption of MB dye on WSAC2-900 at 299 K

Sample	WSAC2-900	
Langmuir isotherm	R_L	0.0029
	q_m (mg/g)	552.4851
	K_L	0.6053
	R^2	0.9993
Freundlich isotherm	$1/n$	0.0622
	k	409.4721
	R^2	0.9015
Temkin isotherm	A (L/g)	28.7332
	A_T	2846497.9315
	b	86.5162
	R^2	0.8900
D-R isotherm	β (mol ² /J ²)	-3.0726×10^{-7}
	q_m (mg/g)	540.2867
	E (KJ/mol)	4033.8837
	R^2	0.6968

* R_L , the Langmuir separation factor; K_L , Langmuir constant ; $1/n$, Freundlich constant related to the adsorption intensity of biomass activated carbon; k , an empirical constant related to the nature and type of pollutants in the solution and biomass activated carbon; A , A constant relating to the heat of adsorption; A_T , Dimensionless adsorption constant; b : A constant related to the free energy of adsorption; β , Parameters related to the free energy of adsorption; E , Energy per mole of adsorbent.

in nature [78, 79]. The system's ΔG° is negative, indicating that the adsorption process is spontaneous, which is highly beneficial for facilitating the adsorption reaction. Moreover, as the temperature increases, the value of ΔG° slightly decreases, suggesting that temperature does not have a significant impact on the progress of the adsorption reaction. Additionally, the decrease in the Gibbs free energy of the system also indicates that the system is evolving towards

a more stable and lower energy state [80]. These findings collectively validate the effectiveness of WSAC2-900 in adsorbing MB.

3.2.5 Study on regeneration performance

The reusability of biomass char is an important factor in evaluating its application value. To assess the regeneration performance of WSAC2-900 after adsorbing MB, adsorption–desorption cycle experiments were conducted. As shown in Fig. 7f, after the first adsorption, the adsorption capacity and removal rate reached 249.6 mg/g and 99.8%, respectively. With an increase in the number of adsorption cycles, after completing the third adsorption experiment, the adsorption capacity and removal rate decreased to 39.0 mg/g and 15.6%, respectively. This decrease occurred because the active sites on the surface of WSAC2-900 were not completely desorbed, leading to a decrease in the number of available adsorption sites and a lower removal rate. Therefore, the maximum usage cycle for WSAC2-900 is three cycles.

3.2.6 Adsorption mechanism

Figure 8 summarizes the main mechanisms of MB adsorption by WSAC2-900. Based on the zeta potential diagram of WSAC2-900 shown in Fig. 4b, it can be inferred that when the pH of the MB solution is greater than the pH_{pzc} , electrostatic interactions are the primary adsorption mechanism. Electrostatic force adsorption is mainly derived from the interaction between oxygen-containing functional groups in WSAC2-900 and cationic MB [56]. When the pH of the MB solution is below the pH_{pzc} , excess H^+ competes with MB cationic groups for limited adsorption sites, leading to a reduction in the electrostatic interactions between WSAC2-900 and the cationic dye. At this point, noncovalent

Table 3 Comparison of the adsorption capacities of different adsorbents for MB

Adsorbent	T (K)	pH	Adsorption capacity q_{max} (mg/g)	Ref.
Sugarcane bagasse waste	303	8	136.5	[59]
Mustard straw	-	-	198	[60]
Eucalyptus wood-based magnetic	328	-	228.22	[25]
Hops	295	6	328.75	[61]
Pinewood	-	-	144	[62]
Caraway seeds	296	-	296	[63]
Date palm	298	8	666	[4]
Bamboo-based	298	11	67.46	[64]
Walnut shell (ZnCl ₂)	318	7	632.13	[37]
Raw walnut shell powder	298	6.93	19.99	[30]
Walnut shell(K ₂ CO ₃)	299	8.13	552.48	This work

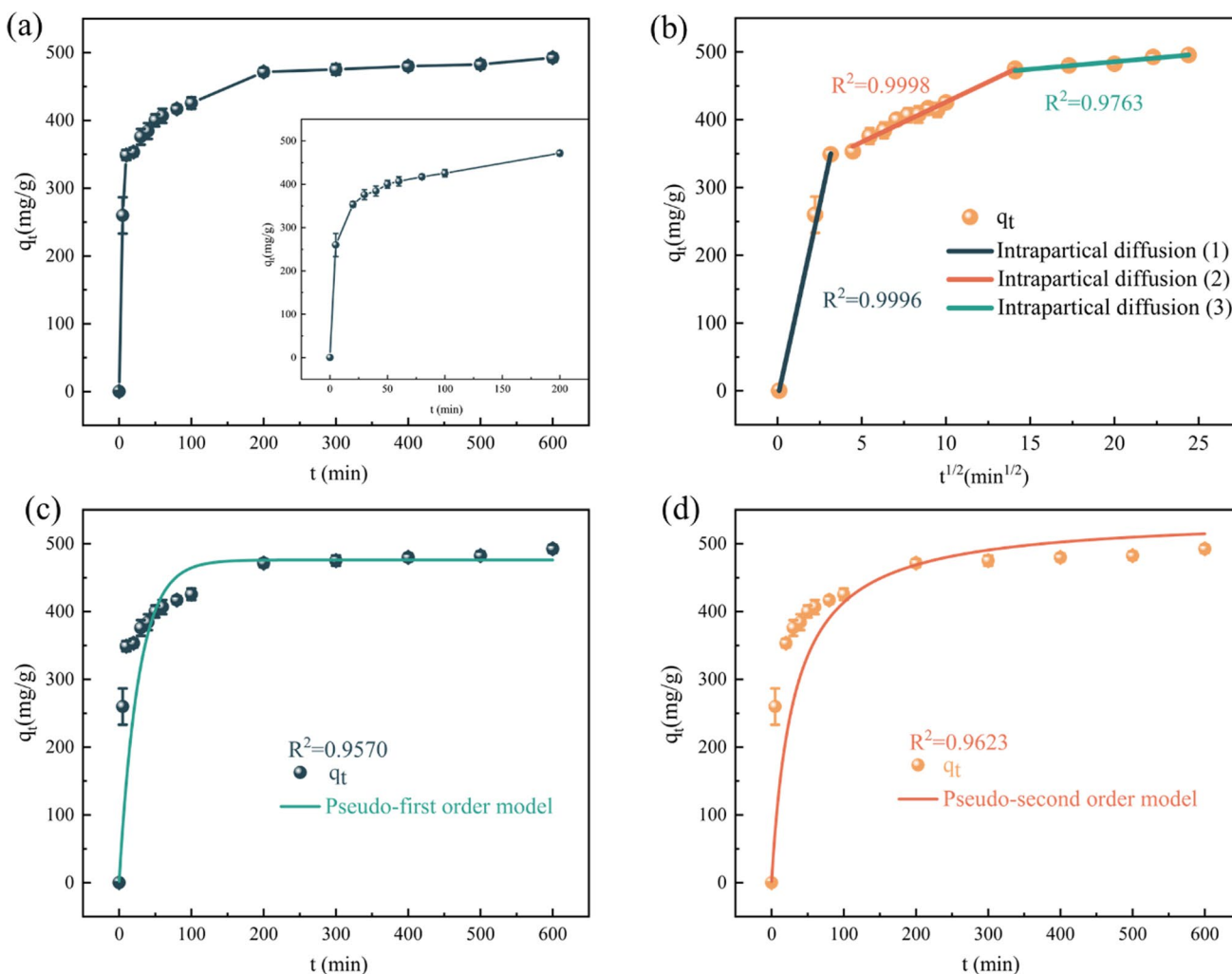


Fig. 6 a The effect of time on the adsorption capacity of WSAC2-900 activated carbon was studied at T = 299 K, 10 mg of adsorbents, 25 ml of adsorbent and pH = 8.13. **b** Fitting curves for intraparticle dif-

fusion of methylene blue adsorption on WSAC2-900 activated carbon. **c** Fitting curves for the pseudo-first-order model and **d** pseudo-second-order model

Table 4 Kinetic parameters of WSAC2-900 adsorption of methylene blue at T = 299 K, 10 mg of adsorbent, 25 ml of adsorbent and pH = 8.13

Sample	Pseudo-first-order model			Pseudo-second-order model		
	$K_1(\text{min}^{-1})$	R^2	$q_e(\text{mg/g})$	$K_2(\text{mg}\cdot\text{g}^{-1}\cdot\text{min}^{-1})$	$q_e(\text{mg/g})$	R^2
WSAC2-900	0.1253	0.9570	462.7037	6.9797×10^{-5}	541.2885	0.9622

Table 5 The adsorption parameters of the diffusion model of WSAC2-900 with adsorbed MB particles at T = 299 K, 10 mg of adsorbent, 25 ml of adsorbent and pH = 8.13

Sample	1st stage			2nd stage			3rd stage		
	K_{1d}	C_1	R^2	K_{2d}	C_2	R^2	K_{3d}	C_3	R^2
WSAC2-900	114.2617	-11.1926	0.9996	11.8203	311.9918	0.9843	2.2293	441.1220	0.9763

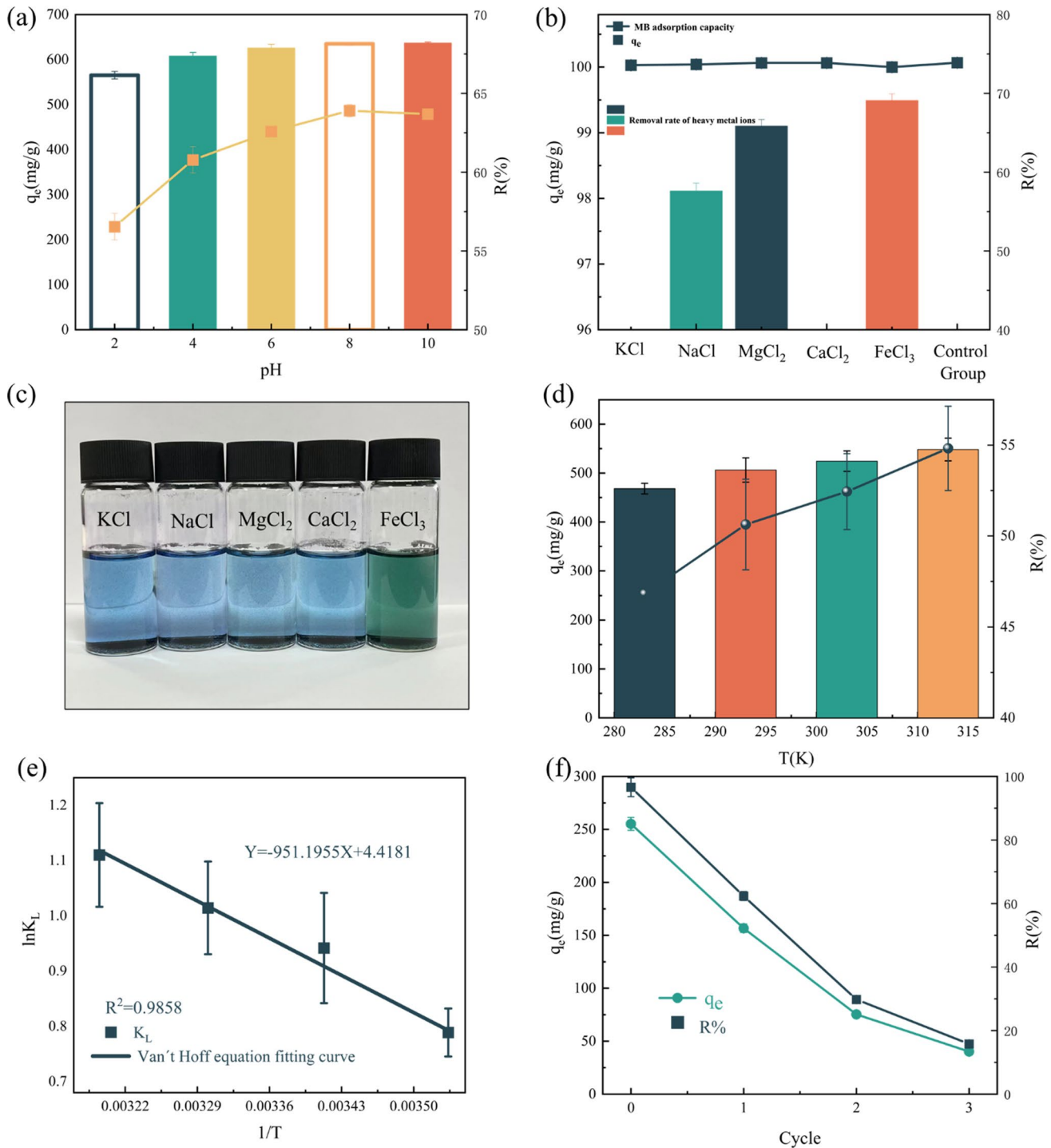
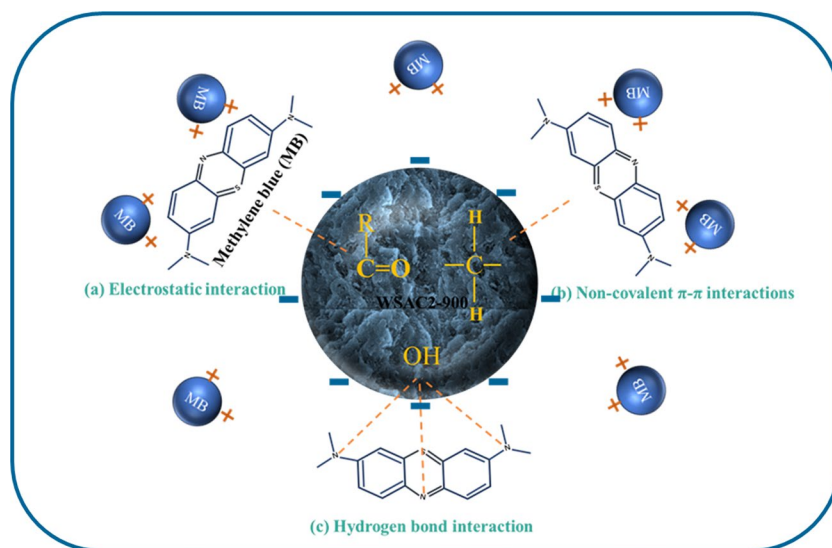


Fig. 7 **a** Influence of pH on the adsorption capacity of WSAC2-900 activated carbon, adsorbent = 10 mg, adsorbent = 25 ml, $T = 299$ K, $pH = 8.13$, and $C_0 = 400$ mg/L. **b** Effect of different cations on MB adsorption by WSAC2-900, adsorbent = 10 mg, adsorbent = 10 ml, $T = 299$ K, $pH = 8.13$, $C_{MB0} = 100$ mg/L, and $C_{M10} = 100$ mg/L. **c** Desorption of adsorbed WSAC2-900 in different metal solutions. **d** Impact of temperature on the adsorption capacity of WSAC2-900

activated carbon at adsorbent = 10 mg, adsorbent = 25 ml, $pH = 8.13$, and $C_0 = 400$ mg/L. **e** Thermodynamic model of methylene blue adsorption by WSAC2-900 activated carbon. **f** Effect of adsorption/desorption cycles on the equilibrium adsorption capacity of MB on MPPMC at adsorbent = 10 mg, adsorbent = 25 ml, $T = 299$ K, $pH = 8.13$, and $C_0 = 100$ mg/L

Table 6 The thermodynamic parameters of MB adsorption on WSAC2-900 at adsorbent =10 mg, adsorbent =25 ml, T = 299 K, pH = 8.13, and C₀ = 400 mg/L were studied

Sample	ΔG° (KJ/mol)				ΔH° (KJ/mol)	ΔS° (J/(mol·K))
	283 K	293 K	303 K	313 K		
WSAC2-900	-1.8558	-2.2936	-2.5549	-2.8887	7.9082	36.7321

Fig. 8 Mechanisms of MB adsorption on WSAC2-900

π - π interactions and hydrogen bonding between methylene (-CH₂-) and hydroxyl (-OH) groups and MB molecules became the dominant binding forces. Hydrogen bonds are formed by the combination of the hydroxyl group on the surface of WSAC2-900 with the N atom of the MB dye, while noncovalent π - π interactions are formed by the combination of the aromatic ring of the MB dye with the hexagonal structure of WSAC2-900 [65]. The entire adsorption process is controlled by various adsorption mechanisms, including van der Waals forces, electrostatic interactions, hydrogen bonding, and noncovalent π - π interactions, with physical adsorption being predominant, accompanied by some degree of chemical adsorption.

4 Conclusions

Walnut shell activated carbon WSAC2-900, prepared with potassium carbonate as an activator, has good adsorption properties for methylene blue. The structure, morphology and surface functional groups of the activated carbon were determined by XRD, nitrogen adsorption/desorption, SEM, FTIR and zeta potential measurements. In the XRD pattern of WSAC2-900 after activation, two broad peaks were detected at $2\theta = 20.64^\circ$ and 43.68° , which are

attributed to the (002) and (100) planes, respectively, of the disordered carbon structure. The specific surface area and pore volume of WSAC2-900 were 1690.9842 m²/g and 0.5963 cm³/g, respectively. SEM images show that the surface of activated carbon is rich in pore structures containing various small channels, which is conducive to the transport of MB molecules and enhances the adsorption capacity. FTIR analysis revealed that -OH, C-H and C=O were involved in the adsorption of MB on the WSAC2-900 surface, and the adsorption process was controlled by van der Waals forces, electrostatic interactions, hydrogen bond interactions and noncovalent π - π interactions. A zeta potential diagram showed that with increasing solution pH, the negative charge of the activated carbon increased, and the adsorption of the cationic dye MB increased. The isotherms, kinetics and thermodynamics of MB adsorption by WSAC2-900 were investigated. The adsorption capacity of MB on WSAC2-900 was 557.5462 mg/g, and the adsorption process was in accordance with a pseudo-second-order kinetic model. At 283 K, 293 K, 303 K and 313 K, the maximum adsorption capacities of MB were 468.1695 mg/g, 506.3057 mg/g, 524.4298 mg/g and 548.2178 mg/g, respectively. Activated carbon can be reused up to three times. In addition, the mechanism of MB adsorption by WSAC2-900 was discussed.

Authors' contributions Gangxin Ren (First Author): Conceptualization, Methodology, Software, Investigation, Formal Analysis, Writing - Original Draft; Zhiyu Li and Peng Fu (Corresponding Author): Data Curation, Supervision.

Funding This work was supported by the National Natural Science Foundation of China (No. 52376199), the Special Project Fund of "Taishan Scholar" of Shandong Province (No. tsqn202103066) and the China Postdoctoral Science Foundation (No. 2021M691969).

Data availability The data that support the findings of this study are available on request from the corresponding author.

Declarations

Ethics approval and consent to participate Not applicable.

Competing interests The authors declare no competing interests.

References

- Solayman HM, Hossen MA, Abd Aziz A et al (2023) Performance evaluation of dye wastewater treatment technologies: a review. *J Environ Chem Eng* 11(3). <https://doi.org/10.1016/j.jece.2023.109610>
- Slama HB, Chenari Bouket A, Pourhassan Z et al (2021) Diversity of synthetic dyes from textile industries, discharge impacts and treatment methods. *Appl Sci* 11(14). <https://doi.org/10.3390/app11146255>
- Amor C, Marchão L, Lucas MS et al (2019) Application of advanced oxidation processes for the treatment of recalcitrant agro-industrial wastewater: a Review. *Water* 11(2). <https://doi.org/10.3390/w11020205>
- Durrani WZ, Nasrullah A, Khan AS et al (2022) Adsorption efficiency of date palm based activated carbon-alginate membrane for methylene blue. *Chemosphere* 302:134793. <https://doi.org/10.1016/j.chemosphere.2022.134793>
- Tang X, Ran G, Li J et al (2021) Extremely efficient and rapidly adsorb methylene blue using porous adsorbent prepared from waste paper: kinetics and equilibrium studies. *J Hazard Mater* 402. <https://doi.org/10.1016/j.jhazmat.2020.123579>
- Shahnaz T, Bedadeep D, Narayanasamy S (2022) Investigation of the adsorptive removal of methylene blue using modified nanocellulose. *Int J Biol Macromol* 200:162–171. <https://doi.org/10.1016/j.ijbiomac.2021.12.081>
- Rathour RKS, Bhattacharya J, Mukherjee A (2019) β -Cyclodextrin conjugated graphene oxide: a regenerative adsorbent for cadmium and methylene blue. *J Mol Liq* 282:606–616. <https://doi.org/10.1016/j.molliq.2019.03.020>
- Albadarin AB, Collins MN, Naushad M et al (2017) Activated lignin-chitosan extruded blends for efficient adsorption of methylene blue. *Chem Eng J* 307:264–272. <https://doi.org/10.1016/j.cej.2016.08.089>
- Allafchian A, Mousavi ZS, Hosseini SS (2019) Application of cress seed mucilage magnetic nanocomposites for removal of methylene blue dye from water. *Int J Biol Macromol* 136:199–208. <https://doi.org/10.1016/j.ijbiomac.2019.06.083>
- Gu Q, Ng TCA, Bao Y et al (2022) Developing better ceramic membranes for water and wastewater Treatment: where microstructure integrates with chemistry and functionalities. *Chem Eng J* 428. <https://doi.org/10.1016/j.cej.2021.130456>
- Xu S, Yan Y, Shuang C et al (2023) Biological magnetic ion exchange resin on advanced treatment of synthetic wastewater. *Bioresour Technol* 372. <https://doi.org/10.1016/j.biortech.2023.128613>
- Zhao C, Zhou J, Yan Y et al (2021) Application of coagulation/flocculation in oily wastewater treatment: A review. *Sci Total Environ* 765. <https://doi.org/10.1016/j.scitotenv.2020.142795>
- Oh M, Lee K, Jeon MK et al (2023) Chemical precipitation-based treatment of acidic wastewater generated by chemical decontamination of radioactive concrete. *J Environ Chem Eng* 11(5). <https://doi.org/10.1016/j.jece.2023.110306>
- Shen Y, Chen N, Feng Z et al (2022) Treatment of nitrate containing wastewater by adsorption process using polypyrrole-modified plastic-carbon: characteristic and mechanism. *Chemosphere* 297. <https://doi.org/10.1016/j.chemosphere.2022.134107>
- Hou M, He Y, Yang X et al (2023) Preparation of biomass biochar with components of similar proportions and its methylene blue adsorption. *Molecules* 28(17). <https://doi.org/10.3390/molecules28176261>
- Kumar JA, Sathish S, Prabu D et al (2023) Agricultural waste biomass for sustainable bioenergy production: feedstock, characterization and pre-treatment methodologies. *Chemosphere* 331:138680. <https://doi.org/10.1016/j.chemosphere.2023.138680>
- Maia LS, da Silva AIC, Carneiro ES et al (2020) Activated carbon from palm fibres used as an adsorbent for methylene blue removal. *J Polym Environ* 29(4):1162–1175. <https://doi.org/10.1007/s10924-020-01951-0>
- Kumar JA, Amarnath DJ, Kumar PS et al (2018) Mass transfer and thermodynamic analysis on the removal of naphthalene from aqueous solution using oleic acid modified palm shell activated carbon. *Desalin Water Treat* 106:238–250. <https://doi.org/10.5004/dwt.2018.22066>
- Sirajo L, Zaini MAA (2023) Iron-loaded coconut shell-activated carbons for orthophosphate adsorption. *Biomass Convers Biorefinery*. <https://doi.org/10.1007/s13399-023-04284-9>
- Oba OA, Pasaogullari Aydinlik N (2022) Preparation of mesoporous activated carbon from novel African walnut shells (AWS) for deltamethrin removal: kinetics and equilibrium studies. *s* 12(7). <https://doi.org/10.1007/s13201-022-01672-w>
- Fodah AEM, Ghosal MK, Behera D (2021) Quality assessment of bio-oil and biochar from microwave-assisted pyrolysis of corn stover using different adsorbents. *J Energy Inst* 98:63–76. <https://doi.org/10.1016/j.joei.2021.06.008>
- Liu Z, Sun Y, Xu X et al (2020) Adsorption of Hg(II) in an Aqueous solution by activated carbon prepared from rice husk using KOH activation. *ACS Omega* 5(45):29231–29242. <https://doi.org/10.1021/acsomega.0c03992>
- Elkholy AS, Yahia MS, Elnwawy MA et al (2023) Synthesis of activated carbon composited with Egyptian black sand for enhanced adsorption performance toward methylene blue dye. *Sci Rep* 13(1):4209. <https://doi.org/10.1038/s41598-023-28556-6>
- Hady AK, Owda ME, Abouzeid RE et al (2023) Harnessing the potential of modified cellulosic pumpkin seed hulls as affordable biosorbents for cationic dye removal from aqueous solutions: adsorption kinetics and isotherm studies. *Biomass Convers Biorefinery*. <https://doi.org/10.1007/s13399-023-05146-0>
- Chen C, Mi S, Lao D et al (2019) Single-step synthesis of eucalyptus sawdust magnetic activated carbon and its adsorption behavior for methylene blue. *RSC Adv* 9(39):22248–22262. <https://doi.org/10.1039/c9ra03490k>
- Supee AH, Zaini MAA (2022) Phosphoric acid-activated bamboo hydrochar for methylene blue adsorption: isotherm and kinetic studies. *Biomass Convers Biorefinery* 14(7):8563–8577. <https://doi.org/10.1007/s13399-022-03465-2>
- Kumar JA, Krithiga T, Narendrakumar G et al (2022) Effect of Ca⁽²⁺⁾ ions on naphthalene adsorption/desorption onto calcium oxide nanoparticle: adsorption isotherm, kinetics and regeneration

- studies. *Environ Res* 204(Pt B):112070. <https://doi.org/10.1016/j.envres.2021.112070>
28. Guo J, Song Y, Ji X et al (2019) Preparation and characterization of nanoporous activated carbon derived from prawn shell and its application for removal of heavy metal ions. *Materials (Basel)* 12(2). <https://doi.org/10.3390/ma12020241>
29. Yang J, Qiu K (2010) Preparation of activated carbons from walnut shells via vacuum chemical activation and their application for methylene blue removal. *Chem Eng J* 165(1):209–217. <https://doi.org/10.1016/j.ccej.2010.09.019>
30. Farch S, Yahoum MM, Toumi S et al (2023) Application of walnut shell biowaste as an inexpensive adsorbent for methylene blue dye: isotherms, kinetics, thermodynamics, and modeling. *Separations* 10(1). <https://doi.org/10.3390/separations10010060>
31. Jawad AH, Mohammed SA, Mastuli MS et al (2018) Carbonization of corn (*Zea mays*) cob food residue by one-step activation with sulfuric acid for methylene blue adsorption. *Desalin Water Treat* 118:342–351. <https://doi.org/10.5004/dwt.2018.22680>
32. Surip SN, Abdulhameed AS, Garba ZN et al (2020) H₂SO₄-treated Malaysian low rank coal for methylene blue dye decolorization and cod reduction: optimization of adsorption and mechanism study. *Surf Interfaces* 21. <https://doi.org/10.1016/j.surf.2020.100641>
33. Musa SA, Abdulhameed AS, Baharin SNA et al (2023) Coal-based activated carbon via microwave-assisted ZnCl₂ activation for Methyl violet 2B dye removal: optimization, desirability function, and adsorption mechanism. *Minerals* 13(3). <https://doi.org/10.3390/min13030438>
34. Jawad AH, Surip SN (2022) Upgrading low rank coal into mesoporous activated carbon via microwave process for methylene blue dye adsorption: Box Behnken Design and mechanism study. *Diam Relat Mater* 127. <https://doi.org/10.1016/j.diamond.2022.109199>
35. Jawad AH, Mehdi ZS, Mohd Ishak MA et al (2018) Large surface area activated carbon from low-rank coal via microwave-assisted KOH activation for methylene blue adsorption. *Desalin Water Treat* 110:239–249. <https://doi.org/10.5004/dwt.2018.22226>
36. Aygün A, Yenisoay-Karakaş S, Duman I (2003) Production of granular activated carbon from fruit stones and nutshells and evaluation of their physical, chemical and adsorption properties. *Microporous Mesoporous Mater* 66(2-3):189–195. <https://doi.org/10.1016/j.micromeso.2003.08.028>
37. Li Z, Hanafy H, Zhang L et al (2020) Adsorption of congo red and methylene blue dyes on an ashitaba waste and a walnut shell-based activated carbon from aqueous solutions: experiments, characterization and physical interpretations. *Chem Eng J* 388. <https://doi.org/10.1016/j.ccej.2020.124263>
38. Chen Z, Xue R, Hou X et al (2023) Multifunctional material integrated from walnut shell-derived porous carbon and Co/Zn-S for high-performance supercapacitors and adsorbents. *Ind Crop Prod* 205. <https://doi.org/10.1016/j.indcrop.2023.117415>
39. Yue L, Rao L, Wang L et al (2018) Efficient CO₂ adsorption on nitrogen-doped porous carbons derived from D-glucose. *Energy Fuel* 32(6):6955–6963. <https://doi.org/10.1021/acs.energyfuels.8b01028>
40. Rao L, Yue L, Wang L et al (2018) Low-temperature and single-step synthesis of N-Doped porous carbons with a high CO₂ adsorption performance by sodium amide activation. *Energy Fuel* 32(10):10830–10837. <https://doi.org/10.1021/acs.energyfuels.8b02659>
41. Cui H, Xu J, Shi J et al (2021) Evaluation of different potassium salts as activators for hierarchically porous carbons and their applications in CO₂ adsorption. *J Colloid Interface Sci* 583:40–49. <https://doi.org/10.1016/j.jcis.2020.09.022>
42. Albatrni H, Abou Elezz A, Elkhatat A et al (2024) A green route to the synthesis of highly porous activated carbon from walnut shells for mercury removal. *J Water ProcEngineering* 58. <https://doi.org/10.1016/j.jwpe.2024.104802>
43. Zhu L, Zhao N, Tong L et al (2018) Structural and adsorption characteristics of potassium carbonate activated biochar. *RSC Adv* 8(37):21012–21019. <https://doi.org/10.1039/c8ra03335h>
44. Song X, Zhang H, Zhang J et al (2023) Removal of Ciprofloxacin from water by a Potassium Carbonate-activated Sycamore Floc-based Carbonaceous Adsorbent: adsorption behavior and mechanism. *Langmuir* 39(15):5323–5332. <https://doi.org/10.1021/acs.langmuir.2c03330>
45. Pang YL, Tan JH, Lim S et al (2021) A state-of-the-art review on biowaste derived chitosan biomaterials for biosorption of organic dyes: parameter studies, kinetics, isotherms and thermodynamics. *Polymers (Basel)* 13(17). <https://doi.org/10.3390/polym13173009>
46. Mostafa AG, Abd El-Hamid AI, Akl MA (2023) Surfactant-supported organoclay for removal of anionic food dyes in batch and column modes: adsorption characteristics and mechanism study. *Appl Water Sci* 13(8). <https://doi.org/10.1007/s13201-023-01959-6>
47. Zhang J, Lu F, He X et al (2023) The adsorption of biogenetic odorants onto activated carbon: adsorption characteristics and impacts of algal organic matter. *Environ Res* 238. <https://doi.org/10.1016/j.envres.2023.117072>
48. Baassou Z, Benmahdi F, Reffas A et al (2024) The effect of impregnation ratio and surface modification on the characteristics and performance of activated carbon derived from *Ficus carica* leaves for Cr(VI) removal. *Biomass Convers Biorefinery*. <https://doi.org/10.1007/s13399-024-05432-5>
49. Serafin J, Dziejarski B, Cruz Junior OF et al (2023) Design of highly microporous activated carbons based on walnut shell biomass for H₂ and CO₂ storage. *Carbon* 201:633–647. <https://doi.org/10.1016/j.carbon.2022.09.013>
50. Mozhiarasi V, Natarajan TS (2022) Bael fruit shell-derived activated carbon adsorbent: effect of surface charge of activated carbon and type of pollutants for improved adsorption capacity. *Biomass Convers Biorefinery* 14(7):8761–8774. <https://doi.org/10.1007/s13399-022-03211-8>
51. Sellaoui L, Gómez-Avilés A, Dhaouadi F et al (2023) Adsorption of emerging pollutants on lignin-based activated carbon: analysis of adsorption mechanism via characterization, kinetics and equilibrium studies. *Chem Eng J* 452. <https://doi.org/10.1016/j.ccej.2022.139399>
52. Sevilla M, Diez N, Fuertes AB (2021) More sustainable chemical activation strategies for the production of Porous Carbons. *ChemSusChem* 14(1):94–117. <https://doi.org/10.1002/cssc.202001838>
53. Long S-J, Si C-D (2022) Integrated gas expansion and activation strategy to prepare shaddock peel-derived nitrogen doped honeycomb carbon for high performance supercapacitor. *J Porous Mater* 29(5):1639–1648. <https://doi.org/10.1007/s10934-022-01278-2>
54. Jawad AH, Abdulhameed AS (2020) Statistical modeling of methylene blue dye adsorption by high surface area mesoporous activated carbon from bamboo chip using KOH-assisted thermal activation. *Energy Ecol Environ* 5(6):456–469. <https://doi.org/10.1007/s40974-020-00177-z>
55. Fan Q, Sun J, Chu L et al (2018) Effects of chemical oxidation on surface oxygen-containing functional groups and adsorption behavior of biochar. *Chemosphere* 207:33–40. <https://doi.org/10.1016/j.chemosphere.2018.05.044>
56. Jawad AH, Saud Abdulhameed A, Wilson LD et al (2021) High surface area and mesoporous activated carbon from KOH-activated dragon fruit peels for methylene blue dye adsorption: optimization and mechanism study. *Chin J Chem Eng* 32:281–290. <https://doi.org/10.1016/j.cjche.2020.09.070>
57. Taleb F, Mosbah M b, Elaloui E et al (2017) Adsorption of ibuprofen sodium salt onto Amberlite resin IRN-78: kinetics,

- isotherm and thermodynamic investigations. *Korean J Chem Eng* 34(4):1141–1148. <https://doi.org/10.1007/s11814-017-0012-6>
58. Foo KY, Hameed BH (2010) Insights into the modeling of adsorption isotherm systems. *Chem Eng J* 156(1):2–10. <https://doi.org/10.1016/j.cej.2009.09.013>
 59. Jawad AH, Abdulhameed AS, Bahrudin NN et al (2021) Microporous activated carbon developed from KOH activated biomass waste: surface mechanistic study of methylene blue dye adsorption. *Water Sci Technol* 84(8):1858–1872. <https://doi.org/10.2166/wst.2021.355>
 60. Patidar K, Vashishtha M (2020) Optimization of process variables to prepare Mesoporous activated carbon from mustard straw for dye adsorption using response surface methodology. *Water Air Soil Pollut* 231(10). <https://doi.org/10.1007/s11270-020-04893-4>
 61. Bazan-Wozniak A, Nowicki P, Pietrzak R (2018) Production of new activated bio-carbons by chemical activation of residue left after supercritical extraction of hops. *Environ Res* 161:456–463. <https://doi.org/10.1016/j.envres.2017.11.041>
 62. De Smedt J, Arauzo PJ, Maziarka P et al (2022) Adsorptive carbons from pinewood activated with a eutectic mixture of molten chloride salts: Influence of temperature and salt to biomass ratio. *J Clean Prod* 376. <https://doi.org/10.1016/j.jclepro.2022.134216>
 63. Paluch D, Bazan-Wozniak A, Nosal-Wiercinska A et al (2023) Removal of Methylene blue and Methyl red from Aqueous Solutions using activated Carbons obtained by chemical activation of Caraway seed. *Molecules* 28(17). <https://doi.org/10.3390/molecules28176306>
 64. Ge Q, Li P, Liu M et al (2023) Removal of methylene blue by porous biochar obtained by KOH activation from bamboo biochar. *Bioresour Bioprocess* 10(1). <https://doi.org/10.1186/s40643-023-00671-2>
 65. Amjah AN, Abdulhameed AS, Jawad AH et al (2023) Activated carbon from noodles food waste via microwave-assisted KOH for optimized brilliant green dye removal. *Biomass Convers Biorefinery*. <https://doi.org/10.1007/s13399-023-04764-y>
 66. Rashid RA, Jawad AH, Ishak MAM et al (2016) KOH-activated carbon developed from biomass waste: adsorption equilibrium, kinetic and thermodynamic studies for Methylene blue uptake. *Desalin Water Treat* 57(56):27226–27236. <https://doi.org/10.1080/19443994.2016.1167630>
 67. Saleh TA (2018) Simultaneous adsorptive desulfurization of diesel fuel over bimetallic nanoparticles loaded on activated carbon. *J Clean Prod* 172:2123–2132. <https://doi.org/10.1016/j.jclepro.2017.11.208>
 68. Jiao X, Guttha Y, Zhang W (2017) Application of chitosan/poly(vinyl alcohol)/CuO (CS/PVA/CuO) beads as an adsorbent material for the removal of Pb(II) from aqueous environment. *Colloids Surf B: Biointerfaces* 149:184–195. <https://doi.org/10.1016/j.colsurfb.2016.10.024>
 69. Bedin KC, Souza IPAF, Cazetta AL et al (2018) CO₂-spherical activated carbon as a new adsorbent for Methylene blue removal: kinetic, equilibrium and thermodynamic studies. *J Mol Liq* 269:132–139. <https://doi.org/10.1016/j.molliq.2018.08.020>
 70. Cheung WH, Szeto YS, McKay G (2007) Intraparticle diffusion processes during acid dye adsorption onto chitosan. *Bioresour Technol* 98(15):2897–2904. <https://doi.org/10.1016/j.biortech.2006.09.045>
 71. El-Gawad HA, Kadry G, Zahran HA et al (2023) Chromium disarmament from veritable Tanneries Sewer water utilizing carbonic rice straw as a Sorbent: optimization and carbonic rice straw characteristics. *Water Air Soil Pollut* 234(10). <https://doi.org/10.1007/s11270-023-06644-7>
 72. Zhu W, Liu J, Li M (2014) Fundamental studies of novel zwitterionic hybrid membranes: kinetic model and mechanism insights into strontium removal. *Sci World J* 2014:485820. <https://doi.org/10.1155/2014/485820>
 73. Mozhiarasi V, Natarajan TS (2022) Bael fruit shell-derived activated carbon adsorbent: effect of surface charge of activated carbon and type of pollutants for improved adsorption capacity. *Biomass Convers Biorefinery*. <https://doi.org/10.1007/s13399-022-03211-8>
 74. Li D, Sun L, Yang L et al (2023) Adsorption behavior and mechanism of modified *Pinus massoniana* pollen microcarriers for extremely efficient and rapid adsorption of cationic methylene blue dye. *J Hazard Mater* 465:133308. <https://doi.org/10.1016/j.jhazmat.2023.133308>
 75. Yao Y, Mi N, He C et al (2020) A novel colloid composited with polyacrylate and nano ferrous sulfide and its efficiency and mechanism of removal of Cr(VI) from water. *J Hazard Mater* 399:123082. <https://doi.org/10.1016/j.jhazmat.2020.123082>
 76. Shaban SM, Aiad I, Yassin FA et al (2019) The tail effect of some prepared Cationic Surfactants on silver nanoparticle preparation and their surface, thermodynamic parameters, and antimicrobial activity. *J Surfactant Deterg* 22(6):1445–1460. <https://doi.org/10.1002/jsde.12318>
 77. Wang L, Zhou Z, Li X et al (2024) Enhanced removal of methylene blue from water by mesopore-dominant biochar from kelp: Kinetic, equilibrium and thermodynamic studies. *Colloids Surf A Physicochem Eng Asp* 688. <https://doi.org/10.1016/j.colsurfa.2024.133652>
 78. Ikeuba AI, Agobi AU, Hitler L et al (2022) Green approach towards Corrosion inhibition of mild steel during acid pickling using Chlorpheniramine: experimental and DFT study. *Chem Afr* 6(2):983–997. <https://doi.org/10.1007/s42250-022-00526-x>
 79. Wu Y, Wu Y, Zhang X (2020) The dissolution behavior and apparent thermodynamic analysis of propacetamol hydrochloride in pure and mixed solvents. *J Chem Thermodyn* 143. <https://doi.org/10.1016/j.jct.2019.106018>
 80. Song X, Wang L a, Ma X et al (2017) Adsorption equilibrium and thermodynamics of CO₂ and CH₄ on carbon molecular sieves. *Appl Surf Sci* 396:870–878. <https://doi.org/10.1016/j.apsusc.2016.11.050>

Publisher's Note Springer Nature remains neutral with regard to jurisdictional claims in published maps and institutional affiliations.

Springer Nature or its licensor (e.g. a society or other partner) holds exclusive rights to this article under a publishing agreement with the author(s) or other rightsholder(s); author self-archiving of the accepted manuscript version of this article is solely governed by the terms of such publishing agreement and applicable law.